Submitted to *Neural Information Processing Systems: Natural and Synthetic*, Nov./Dec. 1995

Responses to Transients in Living and Simulated Neurons

Michael Stiber*, Ricci Ieong*, *and*
José P. Segundo†

Technical Report HKUST-CS95-26
May 1995

* Department of Computer Science
The Hong Kong University of Science & Technology
Clear Water Bay, Kowloon, Hong Kong
stiber@cs.ust.hk
ricci@cs.ust.hk

† Department of Neurobiology
and Brain Research Institute
University of California
Los Angeles, CA, 90024
segundo@neurobio.medsch.ucla.edu

Abstract

This paper is concerned with synaptic coding when inputs to a neuron change over time. Experiments were performed on a living and simulated embodiment of a prototypical inhibitory synapse. Results indicate that the neuron's response lags its input by a fixed delay. Based on this, we present a qualitative model for phenomena previously observed in the living preparation, including hysteresis and dependence of discharge regularity on rate of change of presynaptic spike rate. As change is the rule rather than the exception in life, understanding neurons' responses to nonstationarity is essential for understanding their function.

The Hong Kong
University of Science & Technology

Technical Report Series
Department of Computer Science

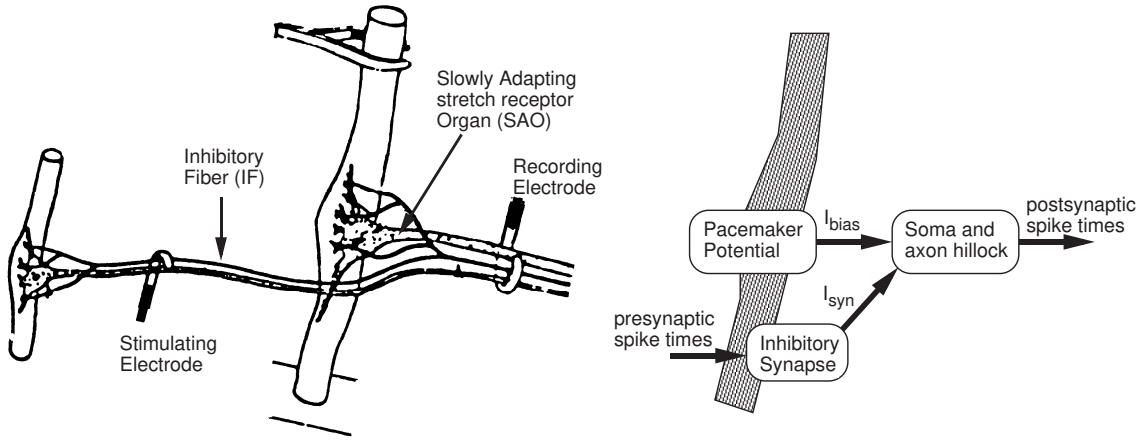

Figure 1: The crayfish stretch receptor experimental setup (left) and the modified permeability model (right).

1 INTRODUCTION

Changes are ubiquitous in nature; survival depends on our ability to cope with them. These changes must necessarily be reflected in changing spike trains of the neurons which encode them, if they are to have any effect on behavior. Despite the importance of neuron transient responses, until recently relatively little has been known about them, except for the aftereffects of abrupt, step-like changes in pacemaker input rates.

This communication continues previous work which involved the crayfish slowly adapting stretch receptor organ: we are concerned with presynaptic discharges with interspike interval *timings* that have *patterns* with trends [7]. These *transients* are among the simplest nonpacemaker input regimes allowing us to examine nonstationary synaptic coding, and are also reasonable models for neural input in sensorimotor systems during motor actions.

Here we expand on experiments in the living preparation with simulations of a physiological neural model. The preparation includes the recognized prototype of an inhibitory synapse, and results obtained from it should be considered valid for any such synapse as a working hypothesis at least [4]. Techniques from the field of nonlinear dynamics are used to explain aspects of synaptic coding that had previously been obscure.

2 A PROTOTYPICAL INHIBITORY SYNAPSE

The living preparation was the crayfish slowly adapting stretch receptor organ; the experimental setup is diagrammed in Fig. 1 (left) [6]. The model shown in Fig. 1 (right) was originally developed by Edman and collaborators to model interspike timing in the

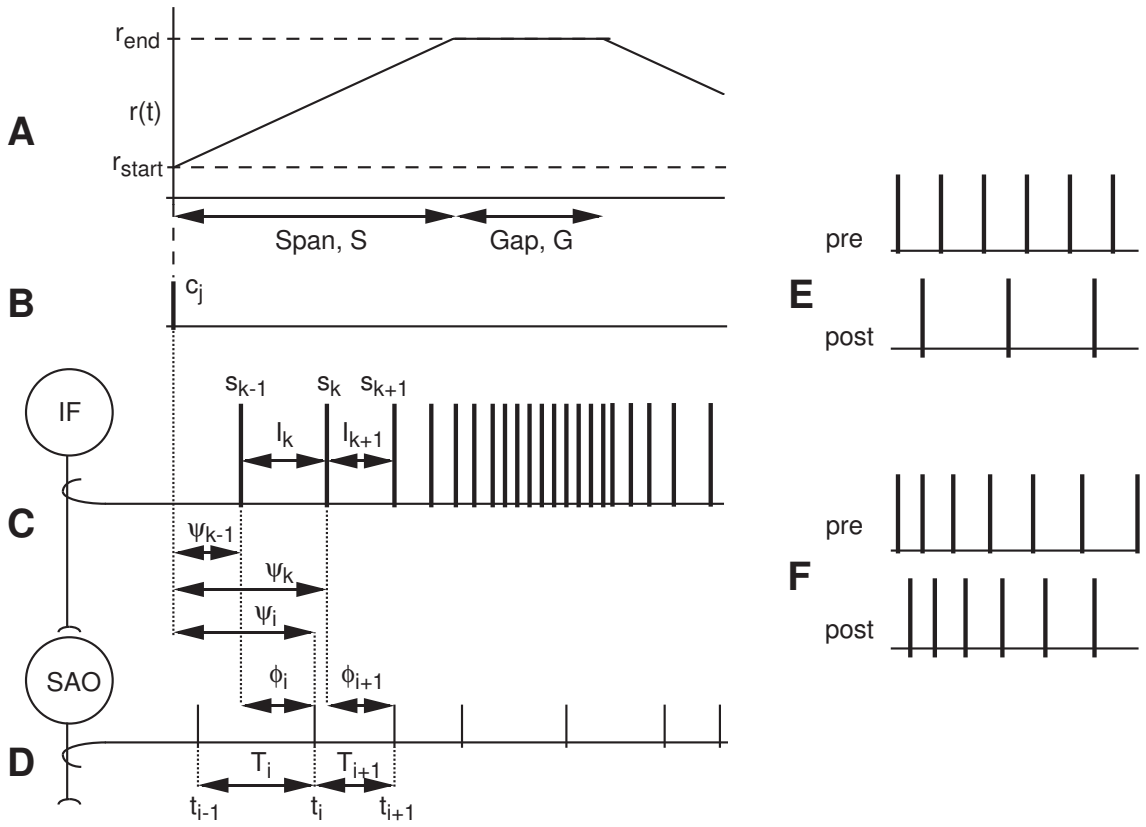

Figure 2: Transient generation and definition of terms.

lobster stretch receptor organs [3]; our simulations assume that inter-species differences are minimal. Model equations are presented in appendix A.

When unperturbed by inputs, a neuron in the organ (referred to as the SAO) and the model both behave as *pacemakers*, firing spontaneously with interspike intervals nearly constant at N, its *natural* interval.

2.1 EXPERIMENTAL METHODS

Transients chosen were those in which the instantaneous input rate (reciprocal of interspike intervals) changed monotonically according to an experimenter-selected waveform (typically a ramp or half-sine). A single experiment involved a series of accelerating and decelerating transients separated by gaps, G, long enough for each transient to be isolated from the aftereffects of the previous one. Fig. 2(A) shows the *rate control waveform*, $r(t)$, for a pair of transients, which determined the desired instantaneous input rate as a function of time. Each transient had a duration or *span*, S, and start and end rates r_{start} and r_{end}.

The times of occurrence of certain events were pertinent. The beginning of each pair of transients was indicated by a *cycle marker*, as in Fig. 2(B), at time c_j. Presynaptic spikes occurred at times s_k (Fig. 2(C)), computed in the simulation by $s_k = s_{k-1} + 1/r(s_{k-1})$. Times of postsynaptic spikes were recorded at times t_i (Fig. 2(D)). $(i, j, k = 0, 1, 2, \ldots)$

Analysis was based on interspike intervals. As shown in Fig. 2(C,D), these were: *presynaptic intervals* $I_k = s_k - s_{k-1}$, *postsynaptic intervals* $T_i = t_i - t_{i-1}$, *phases* $\phi_i = t_i - s_*$ (cross interval from postsynaptic event i back to the most recent preceding presynaptic event), and also *cross intervals* $\psi_k = s_k - c_*$ and $\psi_i = t_i - c_*$ (from a pre- or postsynaptic event back to the most recent preceding cycle marker).

2.2 RESPONSES TO PACEMAKER INPUTS

Previous work has demonstrated what dynamical behaviors arise when one pacemaker neuron inhibits another [6, 8]; we briefly describe one major categorical distinction useful for this treatment.

This distinction is between *periodic* and *aperiodic* behaviors. A periodic behavior in this context is one in which a sequence of intervals $\langle T_i, T_{i+1}, \ldots, T_{i+q-1} \rangle$ and phases $\langle \phi_i, \phi_{i+1}, \ldots, \phi_{i+q-1} \rangle$ repeats unceasingly ($T_i = T_{i+q}$, $\phi_i = \phi_{i+q}$) in the same time as p presynaptic spikes ($pI = qT$, I and T average pre- and postsynaptic intervals, respectively). We call it *p:q locking*, where there are p presynaptic spikes for the q postsynaptic ones in a sequence (p, q integers). Fig. 2(E) schematizes a 2:1 locking (2 presynaptic spikes for each postsynaptic one).

The nonstationary counterpart of this is *p:q alternation*, where there is still a fixed relationship between p pre- and q postsynaptic events, though a trend is now imposed upon the sequence of postsynaptic intervals by the trend of the presynaptic transient. Fig. 2(F) illustrates with a 1:1 alternation and a decelerating presynaptic discharge.

A variety of aperiodic behaviors are produced in response to stationary driving; for brevity's sake, we shall merely note that they have counterparts under transient input.

3 RESPONSES TO TRANSIENTS

The *pooled graphs* in Fig. 3 compare SAO and model responses to a slowly accelerating ramp transient. They show only those intervals or phases whose reference events (i) occurred within the transients' spans, in other words, they are plots of the points (ψ_i, ϕ_i) for $0 \leq \psi_i \leq S$. A pooled graph can be considered a *bifurcation diagram* [1]: a plot of neuron behavior versus a control parameter. In a pooled graph, this control parameter is time since the beginning of the transient, ψ_i, which maps (linearly, in the case of a ramp transient) to instantaneous presynaptic rate.

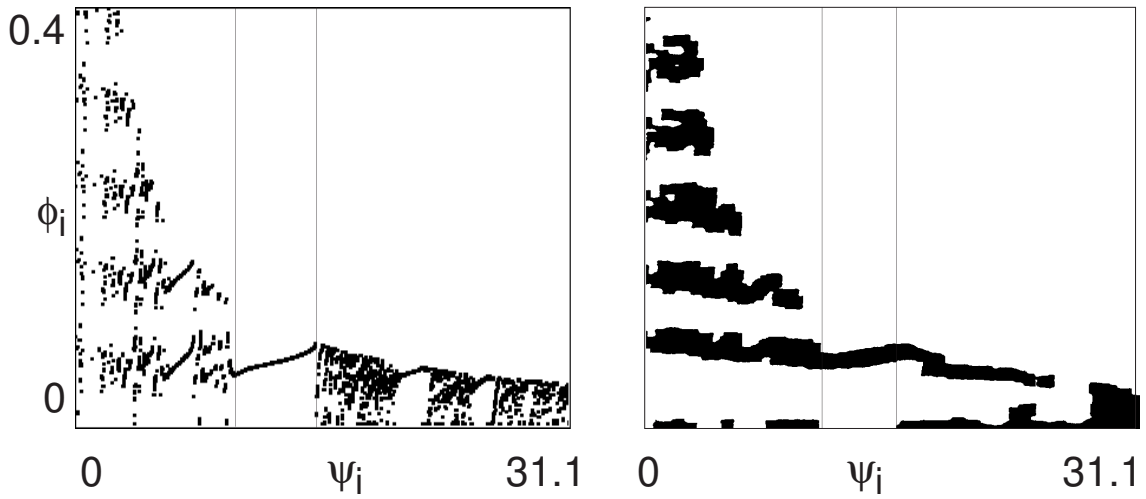

Figure 3: Phase pooled graphs showing transient responses of SAO (right) and simulation (left). Transient was accelerating ramp, 39ms $\leq I_k \leq$ 1.667s, S = 31.1s. Natural firing interval N = 84ms.

In both of the graphs, the plotted points form patterns along the ordinate which change abruptly at certain abscissa values. These values of ψ_i are *bifurcation points*, where qualitatively distinct behaviors some together. For example, in Fig. 3 bifurcation points bounding 1:1 alternation are marked by vertical lines; the alternation itself is revealed by the single category of phases which exists between these two values of ψ_i. Beyond the bifurcation points in either direction lie behaviors other than 1:1 alternation, including non-alternating behaviors and *p*:*q* alternations ($p < q$ to the left of 1:1, $p > q$ to the right).

Generally speaking, the simulation reproduces the major features observed in the SAO, some of which we summarize here briefly:

1. the monotonically changing inputs (when viewed either as instantaneous rates or interspike intervals) are coded into a nonmonotonic output (except under very restricted conditions),

2. transients with the same pattern of spike timings will have different consequences at different average rates,

3. there is a clear correspondence between the bifurcations under transient driving and those resulting from pacemaker driving,

4. behaviors are arranged along the abscissa in the same order as along the rate scale for stationary driving, and

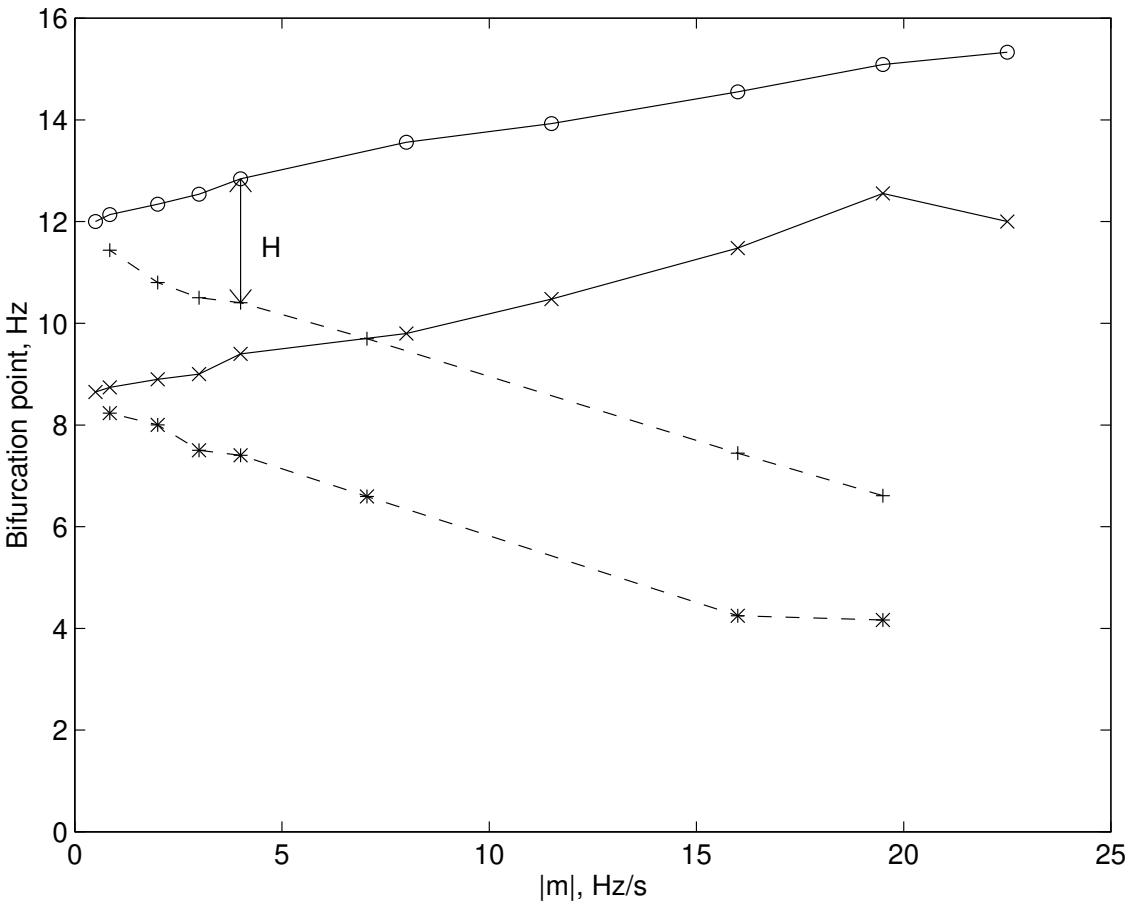

Figure 4: Bifurcation points bounding 1:1 alternation for accelerating (solid lines) and decelerating (dashed lines) transients. Hysteresis (H) caused by non-coincident bifucations.

5. the exact location of bifurcation points between behaviors, and the existence of some of the behaviors, depends on the sign and magnitude of the *slope*, $m = \mathrm{d}r(t)/\mathrm{d}t$ of the input transient ($= \pm$constant for ramp transients).

This final point is one which we shall investigate is somewhat more detail. The SAO's responses to accelerating versus decelerating transients demonstrates *hysteresis*: the instantaneous rate at which it switches between two behaviors (the bifurcation point) for accelerating inhibitory transients is greater than that for their mirror image decelerating ones. This had previously been attributed to the neuron behaving approximately as a "first order lead-lag" system [7]. We can test this hypothesis with the simulation by changing the slope and examining how specific bifurcation points' locations change.

Fig. 4 shows the bifurcation points bounding 1:1 alternation for accelerating and decel-

erating ramp transients plotted versus $|m|$ for the simulation. As slopes increase, points' locations on the rate scale increase for accelerating transients and decrease for decelerating ones. The curves are reasonably well fit by straight lines.

4 DISCUSSION

Before discussing the variation of the neuron's behavior as transients become more abrupt, it is important to reiterate the fact that the well-known nonlinear nature of synaptic coding is manifested here in the nonmonotonic responses of both the SAO and the model to smooth, monotonically changing input transients. This is a consequence of the *bifurcation behavior* of general nonlinear dynamical systems, and does not rely on any special features of the neuron or the model.

For slowly-changing, gradual transients ($|m|$ small), the responses of the SAO or model approximate the global behavior observed under stationary driving within the same range of input rates. As $|m|$ increases, however, the neuron's responses increasingly depart from the stationary bifurcation behaviors, showing dependence on the magnitude of the rate of change of input rate and asymmetric postsynaptic sensitivity to its sign (hysteresis). Behaviors still correspond to stationary ones (low-ratio alternations being the most easily compared), but some of the stationary ones are lost. The boundaries between the remaining ones, while retaining the same ordering along the input rate scale, shift their location.

As shown in Fig. 4, the bifurcation points' shifts are roughly linear functions of $|m|$. This shift can be attributed to the neuron's internal state lagging the input by some fixed delay, as the delay induced by the neuron is the slope of the curves in the figure. A detailed analytical and empirical investigation of the bifurcation point shifting is currently in progress.

Shifting of the bifurcation points can also explain the observed hysteresis and the abolishing of some stationary behaviors. This is perhaps most easily visualized using a Z^n (or *staircase*) formulation: a generalization of the "ZZ-switch" hysteresis curve [2], represented schematically in Fig. 5. In this figure, each "tread" of the staircase corresponds to a family of qualitatively similar neural behaviors, the "risers" are the bifurcations from one behavior type to the next, and the horizontal axis is input rate. As the input rate changes monotonically, the system will shift from one tread to the next as the rate moves past each tread's edge.

For stationary driving, the risers form right angles to the treads. As $|m|$ increases, the "tops" of the risers move to the right, and the "bottoms" move to the left, resulting in each tread overlapping the one below it (as shown in the figure). The amount of shift is described by the curves in Fig. 4. Thus, hysteresis is the result of the difference between riser tops and bottoms: with acceleration, the system's shifts are determined by the tops; with deceleration, by the bottoms. Furthermore, the amount of tread overlap can explain

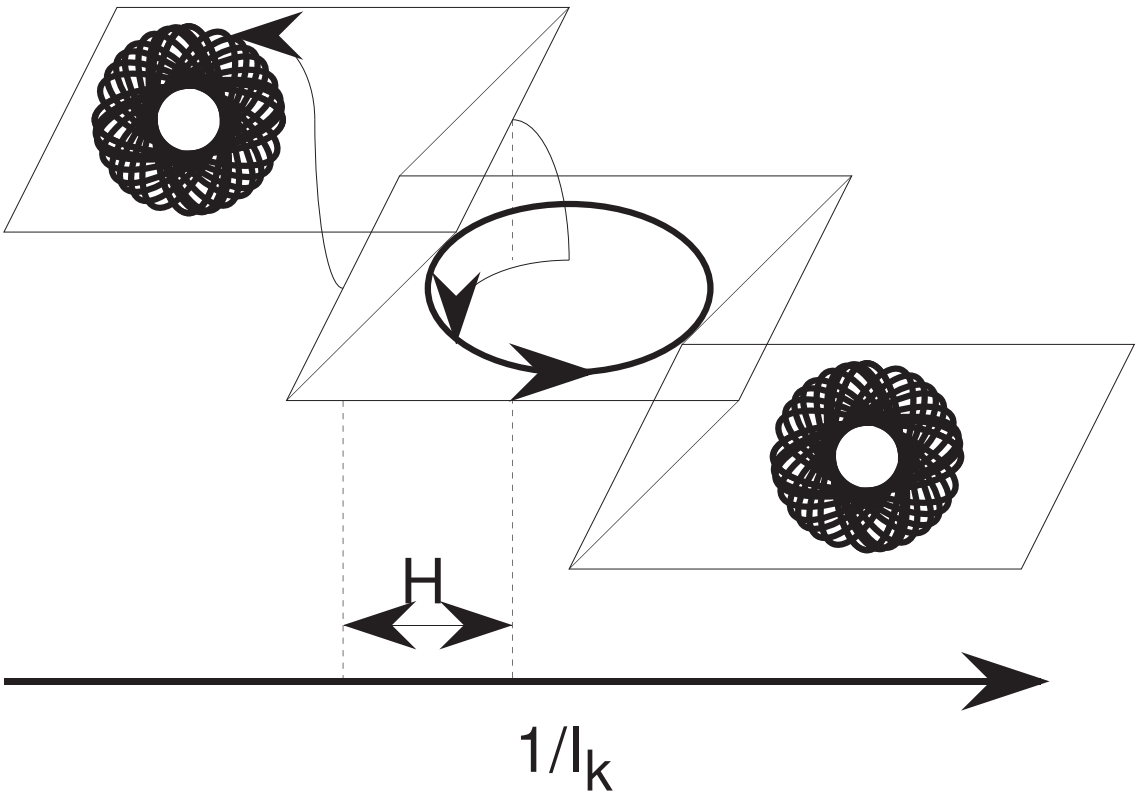

Figure 5: Hysteresis (H) and bifurcation staircase curve for one value of $|m| > 0$, showing 1:1 alternation and neighboring behaviors.

how behaviors are abolished via two mechanisms:

1. if one tread completely overlaps the next, then the system will "skip it",
2. even if complete overlap doesn't occur, the residence time of the system on a tread may be insufficient for its state to approach the dynamical attractor which defines that behavior.

Though still preliminary, it is important to note that this formulation does not depend on the exact quantitative relationship in Fig. 4; *any* nonlinear system which has an internal state that lags changing inputs by at least a constant delay should be expected to exhibit similar responses. This is perhaps the most important take-home message for neural coding: it is but one manifestation of *universal* principles.

Acknowledgements

The authors would like to thank Dominic Lai and NG Ka Ho for their help in this project. Support for this work was provided by the Hong Kong Research Grants Council (CERG HKUST187/93E). Mike would like to thank Bilin for her interference, er, I mean, help.

References

[1] P. Bergé, Y. Pomeau, and C. Vidal, *Order Within Chaos: A Deterministic Approach to Turbulence*. New York: Wiley, 1986.

[2] B. Deng, "Constructing homoclinic orbits and chaotic attractors," *Int. J. Bifurcation and Chaos*, vol. 4, no. 4, pp. 823–41, 1994.

[3] A. Edman, S. Gestrelius, and W. Grampp, "Analysis of gated membrane currents and mechanisms of firing control in the rapidly adapting lobster stretch receptor neurone," *J. Physiol.*, vol. 384, pp. 649–69, 1987.

[4] S. W. Kuffler and C. Eyzaguirre, "Syanptic inhibition in an isolated nerve cell," *J. Gen. Physiol.*, vol. 39, no. 1, pp. 155–84, 1955.

[5] K. Ozawa and K. Tsuda, "Membrane permeability change during inhibitory transmitter action in crayfish receptor cell," *J. Neurophysiol.*, vol. 36, no. 5, pp. 805–16, 1973.

[6] J. P. Segundo, E. Altshuler, M. Stiber, and A. Garfinkel, "Periodic inhibition of living pacemaker neurons: I. Locked, intermittent, messy, and hopping behaviors," *Int. J. Bifurcation and Chaos*, vol. 1, pp. 549–81, September 1991.

[7] J. Segundo, M. Stiber, E. Altshuler, and J.-F. Vibert, "Transients in the inhibitory driving of neurons and their post-synaptic consequences," *Neuroscience*, vol. 62, no. 2, pp. 459–80, 1994.

[8] M. Stiber and J. P. Segundo, "Dynamics of synaptic transfer in living and simulated neurons," in *IEEE International Conference on Neural Networks*, (San Francisco), pp. 75–80, 1993.

A PERMEABILITY MODEL EQUATIONS

The model represents ionic fluxes regulated by the membrane permeabilities P_{Na}, P_{K}, $P_{\mathrm{L,Na}}$, $P_{\mathrm{L,K}}$, and $P_{\mathrm{L,Cl}}$, for Na^+, K^+, and 3 leakage channels, respectively. There are also two pumping pathways, $I_{\mathrm{p,Na}}$ and $I_{\mathrm{p,K}}$, the generator bias current, I_{bias}, and I_{syn} (inputs

from the presynaptic cell cause fixed-duration changes in the synaptic permeability, P_{syn}, to Cl^-[5]). The membrane potential equation is presented in (1), where the currents I_{X} (for type X) are shown in (2) through (6).

$$\mathrm{d}V_m/\mathrm{d}t = -(I_{\mathrm{Na}} + I_{\mathrm{K}} + I_{\mathrm{L,Na}} + I_{\mathrm{L,K}} + I_{\mathrm{L,Cl}} + I_{\mathrm{p}} + I_{\mathrm{bias}} + I_{\mathrm{syn}})/C_m \tag{1}$$

$$I_{\mathrm{Na}} = A\bar{P}_{\mathrm{Na}} m^2 h l \frac{V_m F^2}{RT} \frac{[\mathrm{Na}^+]_o - [\mathrm{Na}^+]_i \exp(FV_m/RT)}{1 - \exp(FV_m/RT)} \tag{2}$$

$$I_{\mathrm{K}} = A\bar{P}_{\mathrm{K}} n^2 r \frac{V_m F^2}{RT} \frac{[\mathrm{K}^+]_o - [\mathrm{K}^+]_i \exp(FV_m/RT)}{1 - \exp(FV_m/RT)} \tag{3}$$

$$I_{\mathrm{syn}} = A\bar{P}_{\mathrm{syn}} \frac{V_m F^2}{RT} \frac{[\mathrm{Cl}^-]_o - [\mathrm{Cl}^-]_i \exp(-FV_m/RT)}{1 - \exp(-FV_m/RT)} \times \sum_{k=1}^{K} \left(e^{(s_k - t)/\tau_+} - e^{(s_k - t)/\tau_-} \right) \tag{4}$$

$$I_{\mathrm{L,X}} = AP_{\mathrm{L,X}} \frac{V_m F^2}{RT} \frac{[X]_o - [X]_i \exp(FV_m/RT)}{1 - \exp(FV_m/RT)} \tag{5}$$

$$I_{\mathrm{p}} = \frac{AF}{3} \frac{\bar{J}_{\mathrm{p,Na}}}{\left(1 + \frac{K_m}{[\mathrm{Na}^+]_i}\right)^3} \tag{6}$$

Here A is the cell membrane area, the $\bar{P}_{\mathrm{X}}$ are the maximum permeabilities, F is the Faraday constant, R the universal gas constant, T absolute temperature, k a counter of IPSPs, s_k time of arrival of IPSP k, and m, h, l, n, and r are gating variables. The variables m, h, and l are the fast activation, fast inactivation, and slow inactivation, respectively, for P_{Na}. For P_{K}, n is fast activation, and r is slow inactivation. Gating variables are governed by first-order kinetics. The pumping mechanism exchanges 3 Na^+ ions for 2 K^+ in equation (6), where $\bar{J}_{\mathrm{p,Na}}$ is the maximum Na^+ pump capacity, K_m is a constant, and the factor of 1/3 is the net effect of the 3:2 pump ratio. For our purposes, $[\mathrm{Cl}^-]_i$, $[\mathrm{K}^+]_i$, and $[\mathrm{Na}^+]_i$ are assumed constant.